Technical Notes

Slotted rotatable target assembly and systematic error analysis for a search for long range spin dependent interactions from exotic vector boson exchange using neutron spin rotation

C. Haddock [c,*], B. Crawford [d], W. Fox [a], I. Francis [f,1], A. Holley [e], S. Magers [d], M. Sarsour [b], W.M. Snow [a], J. Vanderwerp [a]

[a] Indiana University/CEEM, 2401 Milo B Sampson Lane, Bloomington, IN 47408, USA
[b] Georgia State University, Atlanta, GA 30303, USA
[c] Nagoya University, Furocho, Chikusa Ward, Nagoya, Aichi Prefecture 464-0814, Japan
[d] Gettysburg College, 300 N Washington St, Gettysburg, PA 17325, USA
[e] Tennessee Tech University, 1 William L Jones Dr, Cookeville, TN 38505, USA
[f] 612 S Mitchell St Bloomington, IN 47401, USA

A B S T R A C T

We discuss the design and construction of a novel target array of nonmagnetic test masses used in a neutron polarimetry measurement made in search for new possible exotic spin dependent neutron–atom interactions of Nature at sub-mm length scales. This target was designed to accept and efficiently transmit a transversely polarized slow neutron beam through a series of long open parallel slots bounded by flat rectangular plates. These openings possessed equal atom density gradients normal to the slots from the flat test masses with dimensions optimized to achieve maximum sensitivity to an exotic spin-dependent interaction from vector boson exchanges with ranges in the mm - μm regime. The parallel slots were oriented differently in four quadrants that can be rotated about the neutron beam axis in discrete 90° increments using a Geneva drive. The spin rotation signals from the 4 quadrants were measured using a segmented neutron ion chamber to suppress possible systematic errors from stray magnetic fields in the target region. We discuss the per-neutron sensitivity of the target to the exotic interaction, the design constraints, the potential sources of systematic errors which could be present in this design, and our estimate of the achievable sensitivity using this method.

Published by Elsevier B.V.

Over the last decade a growing number of experiments have sought new interactions of Nature with weak couplings and force ranges at the mm-μm scale. Such exotic interactions might arise from string theory, from pseudo-Goldstone bosons generated by spontaneous symmetry breaking at high energy scales, from the as-yet-unknown physics behind dark energy, etc. A detailed review on the state of this developing subfield can be found in [1,2].

A general classification of the potentials that can exist between nonrelativistic fermions (protons, neutrons, and electrons in our case) from the nonrelativistic limit of a single spin 0 or spin 1 boson exchange assuming only rotational invariance [3] uncovered 16 different operator structures at first order involving the spins, momenta, interaction range, and various possible couplings of the particles. This is a small enough number of distinct possibilities that it has motivated many experimentalists to design specific experiments to look for each type. The simple Yukawa interaction of range λ_c is the only spin-independent one on the list. The rest contain Yukawa terms which set the distance scale for the interaction but also depend on the spins of one or both of the fermions.

Low energy neutrons are a particularly useful probe for new possible spin dependent interactions at the mm-μm scale, which could be mediated by a spin-1 boson whose mass m_0 is related to this distance scale λ_c through the relation $m_0 = \frac{\hbar}{\lambda_c c}$, where $\hbar$ is the reduced Planck constant and c is the speed of light in vacuum. Slow neutrons can be polarized with high efficiency and manipulated with delicate precision to conduct sensitive interferometric measurements of many types. Such measurements can be used to place limits on the strength of new possible exotic couplings between ordinary matter.

We sought to measure the possible neutron–atom axial vector coupling given below in (1):

$$V_5 = \frac{g_A^2 \hbar^2}{4\pi m_n} \frac{e^{-r/\lambda}}{r} \left(\frac{1}{r} + \frac{1}{\lambda_c} \right) \vec{\sigma} \cdot \left(\frac{\vec{v}}{c} \times \frac{\vec{r}}{r} \right). \tag{1}$$

In this expression g_A is the axial coupling constant, r is the distance between the neutron and the atom, v is the relative velocity, σ is the neutron spin, and m_n is the neutron mass. This interaction potential

---

* Corresponding author.
  E-mail address: cchaddoc@indiana.edu (C. Haddock).
  [1] This is the author's personal address.

induces a rotation of the spin about the $\vec{v} \times \vec{r}$ axis in a way similar to a magnetic field. One can express the effect of this potential in terms of a pseudomagnetic field, which if integrated over a semi-infinite plane is given by

$$B_{AA} = \frac{1}{\gamma_n} \frac{g_A^2}{4} N \frac{\hbar c}{m_n c^2} \lambda_c (\vec{v} \times \hat{y}) e^{-\Delta y / \lambda}, \tag{2}$$

where λ_c is the range of the force and the y direction is normal to the face of the semi-infinite slab.

The first attempt to search for this exotic neutron–atom axial vector coupling at interaction length scales below 1 cm was made by Florian M. Piegsa and Guillaume Pignol at the Paul Scherrer Institute in Switzerland [4]. In their experiment the phase shift from this exotic interaction was sought by comparing the neutron phase shift difference from two parallel subbeams at a series of different distances from the same source (a copper plate in their case) and with the source placed close to one subbeam, with the other subbeam serving as a reference. The measurement used the well-known Ramsey method of separated oscillatory fields and was therefore a quantum interference experiment with a phase shift proportional to the integral of the exotic interaction energy between the neutron and the atoms in the slab. In neither subbeam do the neutrons touch the test mass surface. This approach renders the measurement insensitive to possible sources of systematic error from magnetic field drifts, thermal drifts which change the apparatus geometry, and the magnetic susceptibility of the test mass and has the advantage that it can fit for the known distance dependence of the exotic interaction. Possible systematic errors from magnetic impurities in the sample can be dealt with by measurements of the residual magnetic field from the sample. The sub-mm distance scales of interest for the exotic interaction search of interest dictates the choice of various aspects of the geometry.

The number of neutrons used in the pioneering Piegsa and Pignol experiment was small and limited by their choice of a single planar source mass. We sought to improve upon this experiment by increasing the total number of neutrons used to probe the possible spin dependent interaction and to employ polarized neutron spin rotation as the measurement method rather than Ramsey spectroscopy. The brightness of the slow neutron sources available for scientific research at national neutron facilities are all about the same within an order of magnitude or so as that of the PSI source used in their experiment, but many of the beams possess a much larger cross sectional area (as large as 10 cm × 10 cm) than that used by Piegsa and Pignol. However, we cannot take advantage of this full intensity as the potential we are trying to measure has a range of sub-mm scale. Since increasing the width of the beam necessarily increases the average distance between the neutron and slab, doing so quickly reduces the sensitivity to V_5 in the sub-mm range where it is poorly constrained experimentally.

Therefore rather than employing a single slab of material as the V_5 source, we designed a source target which consisted of an array of target slabs designed to maximize a possible V_5 signal. Our multi-slotted target design is an attempt to make efficient use of the large cross sectional area neutron beams which are available and still be able to access possible exotic effects of an interaction with sub-mm range. This mismatch of length scales immediately suggests a parallel multi-slotted target design. As this choice precludes the ability to vary the relative distance between source and subbeams as done by Piegsa and Pignol, we instead choose to surround each neutron subbeam through the target with masses of different densities (glass and copper in this case) and rotate the target so that the sign of the neutron phase shift from the exotic interaction is reversed. This allows us to conduct the search for this exotic interaction in the form of an asymmetry measurement by rotating the target mechanically. In place of the reference beam used by Piegsa and Pignol which is ideally far enough away from the source to feel no exotic interaction, we instead use a set of slots in a different quadrant of the target which are rotated by 90° with respect to the neutron polarization direction. As can be seen from the form of the interaction, this different orientation gives a zero contribution to the

exotic interaction after one averages over the sources. For one of the 4 orientations of the target one therefore gets a null phase shift in two diagonal quadrants and a positive and negative phase shift in the other two diagonal quadrants. One 90° rotation of the target with respect to the beam reverses the positions of the low and high density sources with respect to the neutrons so that, in the absence of systematics, the phase shifts in the zero diagonal quadrants are still zero while the phase shifts in the other pair of diagonal quadrants are reversed. Four 90° rotations of the target cycle all of the test masses through all quadrants of the beam to ensure that there are no effects from target nonuniformities.

In the reminder of this paper we briefly discuss the neutron spin rotation measurement method, the details of the target design used in the experiment, the potential sources of systematic error inherent in this method, and the prospects for improving on the sensitivity of the V_5 search.

1. Neutron spin rotation method

We used a neutron spin rotation polarimeter to search for this interaction, employing a neutron polarimeter described in detail in [5] and shown in Fig. 1. This polarimeter is designed to accept a vertically polarized slow neutron beam and measure the horizontal component of the polarization that can result from a net rotation of the plane of polarization of the neutrons along the neutron beam axis in the magnetically-shielded sample region. This component of the neutron polarization is isolated by a combination of a precession of the neutron spin about a vertical axis in the sample region using an appropriately-tuned magnetic field combined with adiabatic spin transport in a magnetic field of oscillating helicity between the sample region and the neutron polarization analyzer. An earlier version of this polarimeter was used to search for parity violation in neutron spin rotation in ^{4}He [6]. The null result from this experiment was later used to constrain possible exotic parity-odd interactions of the neutron [7] and polarized neutron couplings to in-matter gravitational torsion [8] and in-matter nonmetricity [9].

A slightly modified procedure described below was implemented to search for the neutron spin state change which would be caused by V_5. When a beam of polarized neutrons sent parallel to the surface of a flat slab of nonmagnetic material is subject to the effect of the potential in (1), a rotation of the expectation value of the neutron spin about an axis perpendicular to both the spin and velocity is induced. As mentioned above, this can be understood from nonrelativistic quantum mechanics simply by viewing the cross product term in (1) as a pseudomagnetic field about which the spin expectation value would Larmour precess. In order to measure the asymmetry in the longitudinal polarization state of the neutron spin after it passes through near a target slab we employ a two step process (see Fig. 2). Once the neutron has accumulated an asymmetry from V_5 we rotate the polarization state by $\pi/2$ rad about the vertical ($+y$) axis using a constant magnetic field. We then rotate this new polarization state by $\pm\pi/2$ rad about the longitudinal axis using the adiabatic neutron spin transport field before finally arriving at a polarization analyzer which allows through only neutrons whose polarization vector is pointing along $+\hat{y}$ (see Fig. 1). By computing the difference ratio of the number of neutrons that make it through the analyzer in the + or − state of the adiabatic transport field we can measure an asymmetry which is proportional to the phase shift from the spin coupling of the neutron to the new possible light vector boson of interest.

2. Alternating density gradient scheme

In order to increase the total number of neutron–atom interactions over a polarized slow neutron beam of large cross sectional area while remaining sensitive in the mesoscopic length region of scientific interest, we designed a target using multiple plates containing a large mass density gradient. The test masses must be composed of two plates of
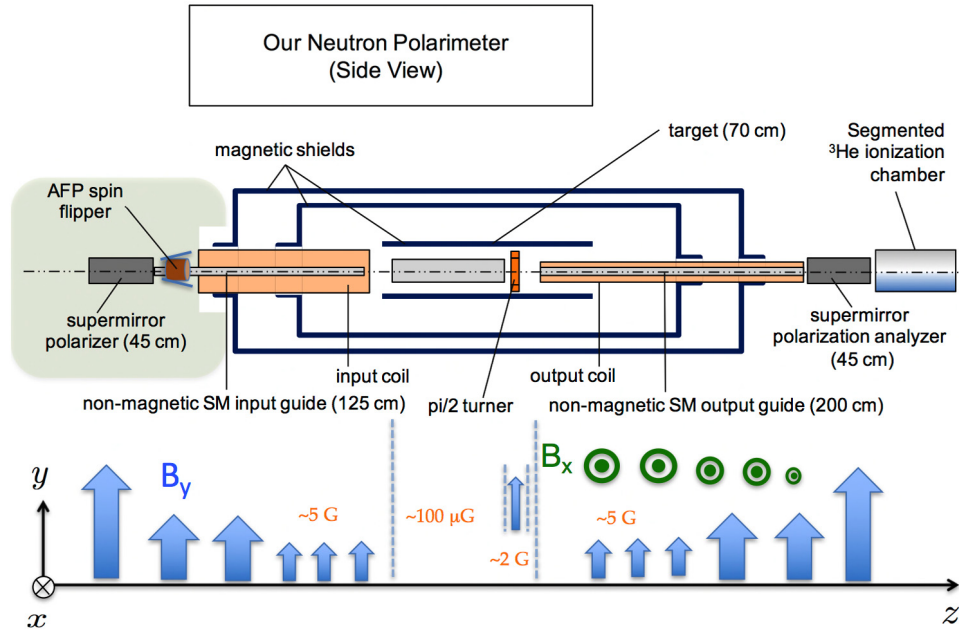
Fig. 1. Diagram of the Polarimeter used to measure the longitudinal polarization asymmetry of the neutrons. This polarimeter is a slightly modified version of that described in [5], where the target in that case is liquid helium and a π-rotation region exists in the center of the target region.
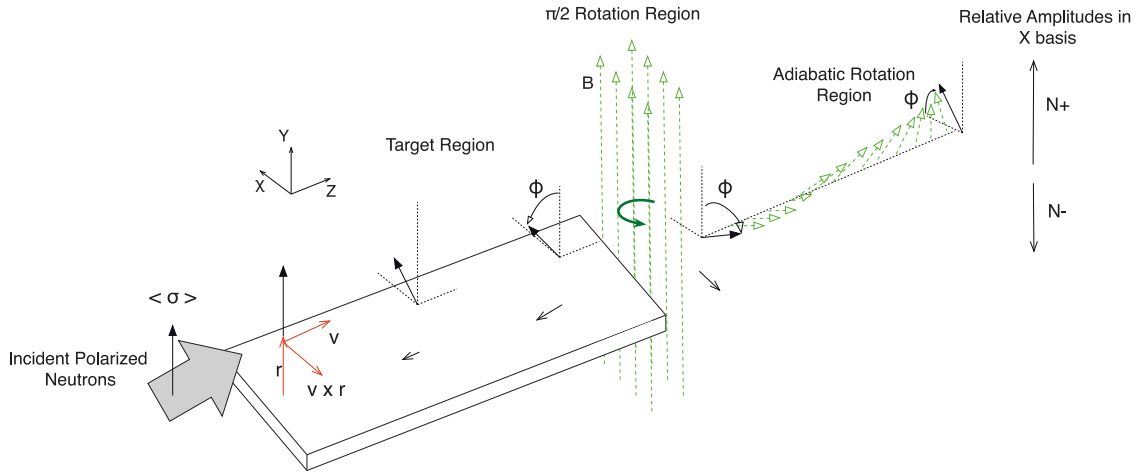

Fig. 2. The rotated spin expectation value is captured and analyzed in a two step process. The "shadow" of the spin vector represents the net polarization asymmetry along a given axis.

different densities. Plates of the same density would create an exact cancellation of any exotic spin-dependent interaction coupling to atom density at the center and a significant reduction near the edges due to the position vector-dependence of the sign of V_5. By using test masses with a large difference in mass density we ensure that the neutron would see a net non-zero V_5 after summing effects from all neutron trajectories between the plates.

Neutron transport simulations were used to investigate the sensitivity of the apparatus to V_5. A simplified geometry of the target was inserted into an existing neutron transport code written for previous experiments with this apparatus studying parity violation in a liquid helium target. The code uses realistic neutron wavelength and angular distributions as well as neutron optical transport. Using (2), the code calculated rotations for all trajectories, including multiple bounces from the target faces, to estimate the strength of the rotation signal and the statistical precision. By varying target materials, thicknesses, neutron index of refraction, and the size of the gap between target faces, a set of viable materials and appropriate configurations was obtained for the phase space of the slow neutron beam at LANSCE, which is similar to that available on most fundamental neutron physics beamlines.

One of the target plates was copper while the other was float glass. The final choice of copper and float glass test masses was based on cost and availability, the low surface roughness of commercially-available materials, the reasonably-sized neutron optical potential of these materials, and on their well-known good neutron optical properties (float glass has been used as backing for neutron supermirrors for decades, and copper was one of the first materials used successfully in early neutron guides). Many of the neutrons passing through the target will bounce from the surfaces of these materials since slow neutrons bounce off sufficiently flat surfaces, therefore, increase the neutron transmission through the device.

The neutron polarimeter used in this work contains a neutron ion chamber at the end of the apparatus which is split into four quadrants and can separately measure the neutron spin rotation angle from each quadrant. The final test mass slabs which fill the target are 50 cm long, 6.5 cm wide and 1.65 mm thick. They are arranged in four quadrant regions each containing eight neutron paths separated by two plate thicknesses. The copper and float glass plates fit into 25 μm tolerance parallel grooves that extend through the target region, as shown in
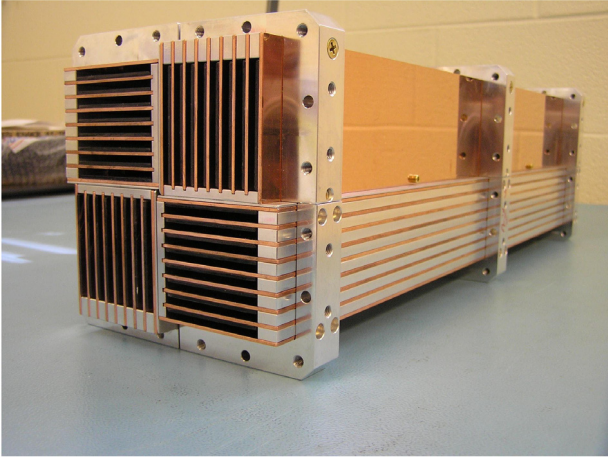
Fig. 3. The copper and float glass target array designed to search for an exotic axial coupling of polarized neutrons to matter. The borated aluminum neutron shielding used to reduce neutron activation of the target materials is not shown.
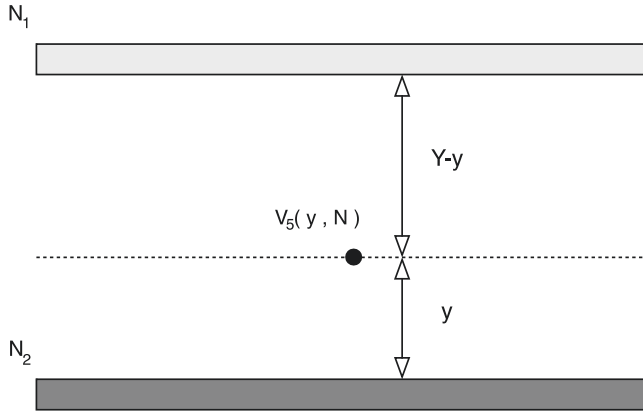

Fig. 4. Procedure for estimating the sensitivity in the air gap between two adjacent target plates using the new target design.

Fig. 3. As a control on the size of rotations due to magnetic fields, two of the quadrants have plates oriented such that $\vec{v} \times \vec{r}$ is in the same direction as the initial neutron spin, in our case vertical. Thus, one expects no fifth force rotation in the quadrants with vertical plates.

We can compare the sensitivity of this neutron beam/target combination with that of the PSI experiment using the expression for the rotation resulting from a neutron passing through the pseudomagnetic field near a slab of material. Using (2) we can find the sensitivity to rotation as a function of g_A^2,

$$\frac{\phi_{PSI}}{g_A^2} = N L \frac{\hbar c}{4 m_n c^2} \lambda_c e^{-\Delta y / \lambda}, \tag{3}$$

where L is the length along which the neutron is in the pseudofield and N is the number density of the target slab. In the PSI experiment a pencil-like beam of approximately 0.3 mm^2 passed beside a 48-cm long, 1.9-cm thick copper slab. For the length scales of interest here the semi-infinite slab approximation is sufficient. For $\lambda_c = \Delta y = 0.1$ cm, we find $\phi_{PSI}/g_A^2 = 5.2 \times 10^{10}$ rad.

For the target described above we can make a similar estimate where neutrons are rotated in opposite directions from different density slabs above and below as shown in Fig. 4. Averaging rotations along the vertical direction, $\frac{1}{Y} \int_0^Y dy$, between semi-infinite slabs separated by distance Y, we obtain

$$\frac{\phi_{NSR}}{g_A^2} = L \frac{\hbar c}{4 m_n c^2} \lambda_c \frac{1}{Y} \int_0^Y \left[N_1 e^{-y/\lambda} - N_2 e^{-y/\lambda} \right] dy, \tag{4}$$

leading to

$$\frac{\phi_{NSR}}{g_A^2} = \frac{L \lambda_c^2}{Y} \frac{\hbar c}{4 m_n c^2} \left(N_1 - N_2 \right) \left(1 - e^{-Y/\lambda_c} \right). \tag{5}$$

Using the values of $L = 50$ cm and $Y = 0.37$ cm, the densities for copper and glass, and $\lambda_c = 0.1$ cm, we find $\phi_{NSR}/g_A^2 = 2.6 \times 10^{10}$ rad, smaller than that obtained using (3) by a factor of two. This approximation is less accurate at longer length scales as the targets no longer appear infinitely thick. To obtain a more realistic value for ϕ_{NSR}/g_A^2 in our more complicated geometry we performed Monte Carlo neutron transport simulations which use numerical solutions of the pseudofield between non-infinite slabs, include all slabs of the current target design, and incorporate the neutron phase space for FP12 at LANSCE. The simulations indicate about the same sensitivity as in the analytical calculation at $\lambda_c = 0.01$ cm, about a factor of three less sensitivity at $\lambda_c = 0.1$ cm and a factor of 8 less sensitivity at $\lambda_c = 0.3$ cm.

For the V_5 length scales of interest in our work our target design has about an order of magnitude less sensitivity per neutron than the PSI experiment depending on the V_5 interaction range of interest. However this is more than compensated by the much larger beam size that this target design enables, which gives an improved statistical sensitivity relative to that experiment by at least a factor of 80, which is the square root of the ratio of the cross sectional areas of the beams transmitted through the target region in both cases. Furthermore this does not take into account additional potential gains in sensitivity from the possible increased neutron density in the beam compared to the PSI experiment.

This design can therefore be used to perform a more sensitive search for V_5 on a large area cold neutron beam. However the additional types of systematic errors which this design can be susceptible to must be analyzed and properly suppressed to take full advantage of the greater potential statistical accuracy. We will discuss the potential sources of systematic error below after giving a detailed description of the target design and operation.

3. Target rotation and state detection

To reduce the effect of possible space-dependent non-uniformities in the background magnetic field as well as possible differences in target plate properties (flatness, thickness, etc.) it was crucial to have a mechanism to rotate the target in discrete, repeatable 90° increments. This would allow neutrons to sample the same region of space with different plates in the same orientation so that an average can be carried out. Additionally by reversing the direction of the mass gradient from quadrant to quadrant we reverse the sign of V_5 between the 4 target states in those quadrants for which V_5 is non zero, as depicted in Fig. 5. Thus, by combining measurements either from different target states or from diagonally opposite quadrants, we can cancel rotations due to magnetic fields while isolating the fifth-force rotations.

In order to consistently reproduce the four target states between rotations about the longitudinal axis we utilized a so-called Geneva Drive mechanism which translates continuous rotation into an intermittent rotary motion like in a mechanical clock. This is done through the use of a rotating cam with a pin which engages a slotted wheel attached to the object to be rotated. The rotation of the object stops as soon as the pin disengages while the cam may continue to rotate independently before engaging another slot, providing the discrete rotation mechanism desired. The rotating cam is driven by an air motor located outside of the outermost magnetic shielding to reduce the amount of magnetic components near the target. Standard lab air at 3×10^5 Pa pressure suffices to rotate the target. The flow to the air motor is controlled by the data acquisition system (DAQ) via an analog relay actuated valve. Each cam cycle rotates the target by 45° and therefore two cycles were required per target state rotation. Target state rotations took 2 s to complete (see Fig. 6).
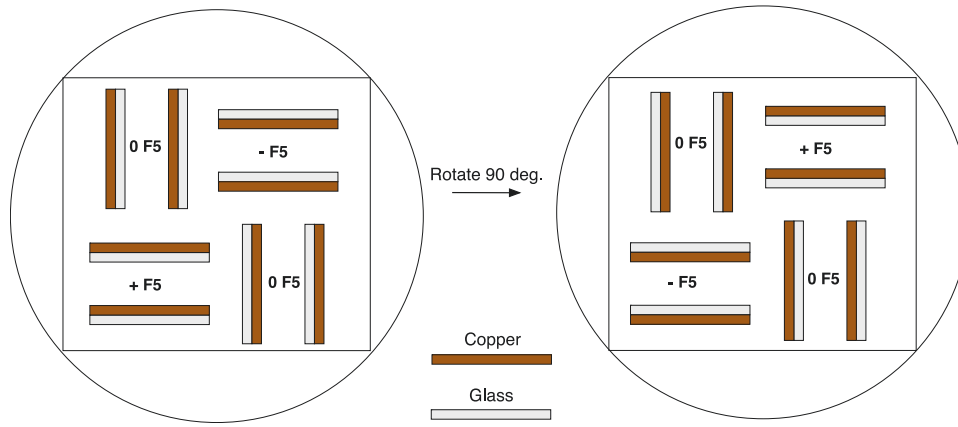
Fig. 5. A face-on simplified schematic of our target design. Neutrons pass through the region between two pairs of copper (brown) and glass (gray) target masses. Our alternating density gradient scheme reverses the sign of the fifth force in each quadrant by rotating the target about its longitudinal axis by 90°. Only 8 of the 32 pairs of test masses are depicted here for clarity. (For interpretation of the references to color in this figure legend, the reader is referred to the web version of this article.)
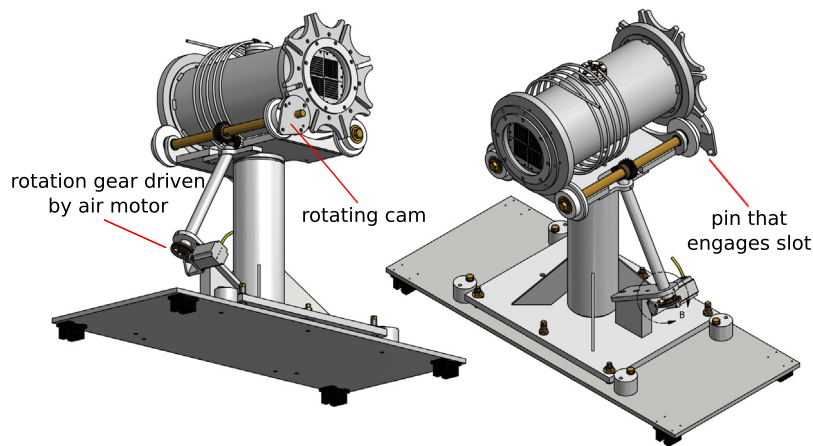

Fig. 6. CAD drawing of Geneva Drive used to rotate target in discrete 45° steps.

To prevent the cam from over or under rotating, it is crucial that we interrupt rotation when the target reaches the desired state. Once the target spends adequate time in the state, the cam will then begin rotation in the same direction as previously to produce the next target state. The target rotation will stop in the next target state using an optical flag interruption scheme. We place an array of three slotted 3 mm transmissive optical sensors below the downstream face of the target such that the slots are parallel to the target face. We fix four plastic optical flags to the target face 90° apart, each with either one, two, or no holes. When the target is not in one of the four desired states infrared light is transmitted to all three receivers from their respective senders and each outputs a non-zero voltage which is sent to the DAQ. The central sensor is always blocked for all four target states and is unblocked during rotation. During the initial fractions of a second when rotation starts, the DAQ ignores the states of the flags while the flags move out of the target position. Then once light transmission to the central sensor is interrupted by the edge of the flag the DAQ waits 0.5 s before stopping rotation. This wait time is long enough to allow the cam to disengage the slotted wheel on the target face but short enough to prevent reengagement from over rotation. Once stopped, data is taken until it is time to rotate to the next target state. Since each flag has a unique arrangement of through holes, the target state can be identified by the DAQ. The DAQ code checks that the registered state is the same as the intended state. If it is not, the DAQ will continue to rotate the target until the intended state is reached. This only occurs at the beginning of a run if the previous run is stopped before the target reaches the usual starting state.

4. Systematic effects

The systematic effects in a search for the V_5 interaction using neutron spin rotation with the target design presented in this paper possess some similarities to the types of systematic errors which have been considered in detail in our previous analysis [5] of parity odd neutron spin rotation for polarized neutron transmission through matter. In both cases the main sources of systematic error come from the presence of residual magnetic fields in the target region coupled with some nonuniformity in the phase space of the neutron beam as it enters into and interacts with the target.

There are two main differences in the sources of systematic errors in these two types of measurements. Whereas for parity-odd neutron spin rotation one is mainly concerned with residual longitudinal magnetic fields, for a V_5 search one must consider systematic effects from both longitudinal and transverse residual magnetic fields in the target region.

In parity-odd neutron spin rotation the beam is transmitted through the target medium, and therefore target-induced nonuniformities in the neutron beam phase space may couple to residual magnetic fields and generate systematic effects. These effects tend to involve refractive neutron optics and small angle scattering, which bend the beam slightly so that it can sample a slightly different residual field in the presence of inevitable spatial gradients and yet still keep the transmitted beam within the phase space acceptance of the neutron polarization analyzer downstream.

In the case of a search for V_5 the beam is transmitted through a ^{4}He gas atmosphere in the target. Small angle scattering, which stays

within the phase space acceptance of the polarimeter, combined with internal magnetic field gradients can generate a systematic error. This systematic error is very similar in character to the liquid helium small angle scattering systematic error described in great detail in [5] and is very small. This systematic is below 1×10^{-7} rad for our assumed internal magnetic field conditions.

We study other systematic effects by looking at the systematic errors which are common between the spin rotation approach to search for V_5 and the approach and implementation of the Piegsa and Pignol measurement:

1. The systematic error from possible magnetic impurities in the test masses is common to both approaches and can be bounded by performing magnetic measurements on the masses. In our target we searched for the presence of residual magnetic fields from the copper and glass plates using a fluxgate magnetometer. We saw no evidence for the presence of any such residual fields at the 10 μG level at a distance of 3 mm from the surfaces of the plates. The resulting upper bound on systematic errors in our measurement from this effect is below 2×10^{-6} rad.

2. The systematic error from the magnetic susceptibility of the test masses, which shifts the value of any residual magnetic field as the mass is moved. This can be suppressed by making the residual magnetic field in the target region as small as possible. Using magnetic shielding it is possible to keep magnetic fields below 1 mG. In our target this susceptibility systematic is different in size from the PSI measurement due to two main effects:

   - It is proportional to the difference in the magnetic susceptibilities of the two materials (copper and glass in our case) on either side of the slots, and
   - It is slightly larger as some of the neutrons in our case bounce from the surface of the test masses and thereby encounter a slightly larger field difference than in the PSI measurement, where the neutron beam never touched the test mass.

   The magnetic susceptibility of both the copper and glass test masses in our target are of the same sign and possess magnitudes that are the same to about a factor of 3 which perturb the magnetic fields at the ppm level (the susceptibility of copper is about $\chi = -10$ ppm and the susceptibility of glass is smaller). This leads to a systematic error in our apparatus of order 1×10^{-4} rad/G if we make the extreme assumption that the neutrons move completely inside the matter. In fact the fraction of the target length that a neutron is inside the copper during a reflection is much smaller than this, and this potential source of systematic error is utterly negligible.

3. Possible systematics from magnetic field drifts are suppressed in slightly different ways in the two designs as discussed above. Both conduct simultaneous null measurements with a reference beam. In the case of our rotating target, however, the simultaneous measurements are conducted on nominally identical but physically distinct test masses. The subsequent target rotations serve to test whether or not there are any nonuniformities in the test mass properties. One 90° rotation of the target with respect to the beam reverses the positions of the low and high density sources with respect to the neutrons, thus removing non-target related rotations such as from stray magnetic fields. Therefore, in the absence of systematics, the phase shifts in the zero diagonal quadrants are still zero while the phase shifts in the other pair of diagonal quadrants are reversed.

In the PSI experiment the neutron beam did not touch the copper test mass. However the beam bounces off the surface of the plates in our design and so we have to consider a different set of systematic errors associated with neutron reflection. We note two potential forms of systematic error which are present in our target design but not in the PSI experiment come from the neutrons bouncing off the test mass surfaces. One comes from the fact that, due to the different neutron indices of refraction of the two test masses, the sections of the neutron phase space transmitted by the target will be very slightly different in the different target positions. This can generate a potential systematic error if these slightly different neutron beam phase space sections see different magnetic fields. This source of systematic error can be suppressed by minimizing both the absolute B fields in the target region and also B field gradients and is discussed in more detail below.

Another potential source of systematic error comes from the very small changes in the neutron beam polarization from neutron spin–orbit scattering from the test masses, which contains the same operator structure as that from the V_5 interaction of interest. The effect on the polarization from neutron spin–orbit scattering is proportional to the neutron momentum transfer q, which, although nonzero for neutron optical reflection from a mirror, is quite small. It is also small because the neutron spin–orbit scattering, which is classically a velocity-dependent effect, leads to an imaginary scattering amplitude, and as the neutron–nucleus scattering amplitude is mainly real in the absence of n-A resonances the neutron spin-dependent component of the interference of the spin–orbit scattering with the potential scattering is a quadratic effect. This latter effect can be calculated using the nice formulae in [10] and is very small in our case: for copper the maximum analyzing power from polarized neutron/copper atom scattering which occurs for momentum transfers corresponding to the critical angle for total external reflection is less than 5×10^{-9} and is therefore completely negligible. Although some neutrons can scatter at higher momentum transfers from the mirrors in the diffuse reflection component of the beam, the intensity of the beam in this component is small compared to the specular component and almost all of the diffusely-reflected neutrons fall well outside the phase space acceptance of the rest of the apparatus. Therefore in the other systematics effects discussed below we will concentrate only on those coming from specular reflection.

To reduce the effects of common-mode magnetic field noise on the neutron spin rotation signal, we arranged the target masses such that different regions of the beam area were made sensitive to possible V_5 signals of opposite sign. By recording these rotation angles simultaneously using a segmented neutron detector we are able to remove the effect of common field noise by taking the difference of these rotation angles. To further reduce systematic effects arising from stray magnetic fields we designed the target to rotate about the beam axis which, due to the arrangement of test masses, changes the sign of V_5 in each region. This allows for a comparison of rotation angles in the same beam phase space at different times, thereby removing the effect of space-dependent background field gradients whereas the aforementioned simultaneous measurement of rotations of opposite sign would remove the effect of time-dependent background field fluctuations.

The spin state changes due to longitudinal or transverse magnetic fields naturally generate different sorts of systematic effects. Longitudinal fields rotate the polarization vector along the axis of the neutron momentum ("left/right" rotations). Transverse magnetic fields rotate the polarization vector forward/backward along the neutron momentum and therefore directly mimic the effect of V_5. Rotations by longitudinal fields before the $\pi/2$ coil are not analyzed by the downstream polarization analyzer but they reduce the polarization product PA by a factor of $\cos \theta_{B_L}$. The $\pi/2$ coil turns forward/backward V_5 rotations into left/right rotations to be analyzed by the analyzing supermirror. Thus, left/right rotations from a longitudinal field after the $\pi/2$ coil add to or subtract from the desired signal and thus can cause false effects. Rotations from transverse fields after the $\pi/2$ coil reduce the PA value by $\cos \theta_{B_T}$.

There are three main effects that can affect the size of a nonzero signal from V_5 in our setup. Nonzero rotations from fringing pseudo-magnetic fields at the edges of vertical-plate quadrants can dilute the signal when subtracting horizontal and vertical quadrants. Magnetic

field gradients which cause slightly different transverse and longitudinal fields in each of the four quadrants can lead to residual rotations after subtracting rotations from different quadrants. A third phenomenon which can both dilute the signal and also lead to a systematic effect comes from "cross-over" neutrons which pass through the target in one quadrant but appear downstream in a different quadrant due to beam divergence in the space between the $\pi/2$ coil and the entrance of the output guide as well as beam transport through the guide (which is split into two separate guide sections with a vertical septum with a supermirror coating on both sides). Rotations from transverse and longitudinal fields from the other three quadrants therefore get mixed into the total rotation of each quadrant. A clean cancellation of magnetic field systematics by doing diagonal averaging/subtraction therefore depends on the amount and symmetry of the signals from these cross-over neutrons as well as the effect of magnetic field gradients.

To analyze the effects of these systematics we present the procedure used to extract the V_5 signal. Let $Q1$, $Q2$, $Q3$, and $Q4$ be the signals in the 4 quadrants of the ion chamber, where we assume a quadrant arrangement with target Sections 1 and 3 possessing horizontal target plates, target sectors 2 and 4 possessing vertical target plates, and the four quadrants starting with 1 in the upper right corner proceed numerically in a counterclockwise direction (see Fig. 5). The rotation angle from V_5 in the horizontal (vertical) target region is given by θ_{HF5} (θ_{VF5}), where θ_{HF5} is the desired signal and θ_{VF5} is a rotation due to fringing of the pseudomagnetic field at the edges of vertical plates. We let θ_{1BTU} (θ_{1BLD}) be the integrated spin rotation angle from the average upstream transverse (downstream longitudinal) field of the first quadrant and similarly for the other three quadrants. To incorporate the possibility of cross-over neutrons, we let a_1, a_2, a_3, and a_4 be the fractions of counts in the different ion chamber quadrants from side-to-side cross-over neutrons originating in the quadrant given by the associated subscripts and b_1, b_2, b_3, and b_4 be the fraction of counts from up-down cross-over neutrons originating in the quadrant given by the associated subscript. Note that quadrants 1 and 4 have opposite $\pi/2$ rotations from quadrants 2 and 3 so θ_{xBTU} changes sign depending on the quadrant. Target quadrants 1 and 3 have opposite target orientations as do target quadrants 2 and 4, so coupled with the $\pi/2$ left/right sign change θ_{HF5} and θ_{VF5} have the same left/right sign, as do θ_{xBLD} as they are downstream from the $\pi/2$ coil. We ignore possible diagonal cross-over neutrons which are negligible by design and in simulations. All angles are assumed to be small enough that we can simply add rotations; this assumption is true for the residual field values we consider. In this case, we get

$$Q1 = \theta_{HF5} + \theta_{1BTU} + \theta_{1BLD} + a_2 \left(-\theta_{2BTU} + \theta_{2BLD} + \theta_{VF5}\right) \tag{6}$$
$$+ b_4 \left(\theta_{4BTU} + \theta_{4BLD} + \theta_{VF5}\right)$$
$$Q2 = \theta_{VF5} - \theta_{2BTU} + \theta_{2BLD} + a_1 \left(\theta_{1BTU} + \theta_{1BLD} + \theta_{HF5}\right)$$
$$+ b_3 \left(-\theta_{3BTU} + \theta_{3BLD} + \theta_{HF5}\right)$$
$$Q3 = \theta_{HF5} - \theta_{3BTU} + \theta_{3BLD} + a_4 \left(\theta_{4BTU} + \theta_{4BLD} + \theta_{VF5}\right)$$
$$+ b_2 \left(-\theta_{2BTU} + \theta_{2BLD} + \theta_{VF5}\right)$$
$$Q4 = \theta_{VF5} + \theta_{4BTU} + \theta_{4BLD} + a_3 \left(-\theta_{3BTU} + \theta_{3BLD} + \theta_{HF5}\right)$$
$$+ b_1 \left(\theta_{1BTU} + \theta_{1BLD} + \theta_{HF5}\right).$$

Now we assume that quadrant differences in the transverse and longitudinal fields are due to linear field gradients in the horizontal and vertical directions, such that the quadrant average of the rotation due to transverse (longitudinal) is given by θ_{BTU} (θ_{BLD}) and is modified by $\pm\delta_H\theta_{BTU}$ ($\pm\delta_V\theta_{BTU}$) due to a horizontal (vertical) gradient for the transverse field, and similarly for the longitudinal field. Thus, the following terms that arise in the next step where we add diagonal

quadrants can be written as

$$\frac{1}{2}\left(\theta_{1BTU} - \theta_{3BTU}\right) = \delta_H\theta_{BTU} + \delta_V\theta_{BTU} \tag{7}$$
$$\frac{1}{2}\left(-\theta_{2BTU} + \theta_{4BTU}\right) = \delta_H\theta_{BTU} - \delta_V\theta_{BTU}$$
$$\frac{1}{2}\left(\theta_{1BLD} + \theta_{3BLD}\right) = \theta_{BLD}$$
$$\frac{1}{2}\left(\theta_{2BLD} + \theta_{4BLD}\right) = \theta_{BLD}.$$

Averaging diagonal quadrants cancels rotations due to the average upstream transverse field and gradients in the longitudinal field:

$$(Q1 + Q3)/2 \tag{8}$$
$$= \theta_{HF5} + \left(\delta_H\theta_{BTU} + \delta_V\theta_{BTU}\right) + \theta_{BLD}$$
$$+ 1/2\left(a_2 + b_2\right)\left(-\theta_{2BTU} + \theta_{2BLD} + \theta_{VF5}\right)$$
$$+ 1/2\left(a_4 + b_4\right)\left(\theta_{4BTU} + \theta_{4BLD} + \theta_{VF5}\right)$$
$$(Q2 + Q4)/2$$
$$= \theta_{VF5} + \left(\delta_H\theta_{BTU} - \delta_V\theta_{BTU}\right) + \theta_{BLD}$$
$$+ 1/2\left(a_1 + b_1\right)\left(\theta_{1BTU} + \theta_{1BLD} + \theta_{HF5}\right)$$
$$+ 1/2\left(a_3 + b_3\right)\left(-\theta_{3BTU} + \theta_{3BLD} + \theta_{HF5}\right).$$

Subtracting the two averages above (8) for data taken at the same time further reduces common mode noise and eliminates rotations from downstream longitudinal fields and the effect of a transverse field horizontal gradient and leaves us with

$$\phi_{diag} = (Q1 + Q3)/2 - (Q2 + Q4)/2 = \tag{9}$$
$$\theta_{HF5} - \theta_{VF5} + 2\delta_V\theta_{BTU}$$
$$- 1/2\left(a_1 + b_1 + a_3 + b_3\right)\theta_{HF5}$$
$$+ 1/2\left(a_2 + b_2 + a_4 + b_4\right)\theta_{VF5}$$
$$+ 1/2\left(a_2 + b_2\right)\left(-\theta_{2BTU} + \theta_{2BLD}\right)$$
$$+ 1/2\left(a_4 + b_4\right)\left(\theta_{4BTU} + \theta_{4BLD}\right)$$
$$- 1/2\left(a_1 + b_1\right)\left(\theta_{1BTU} + \theta_{1BLD}\right)$$
$$- 1/2\left(a_3 + b_3\right)\left(-\theta_{3BTU} + \theta_{3BLD}\right).$$

Here we see the three effects mentioned earlier: the reduction in the θ_{HF5} signal by θ_{VF5} from fringing pseudomagnetic fields in vertical targets, a remaining effect from vertical transverse field gradient, and a number of terms due to neutrons crossing between the four quadrants after the $\pi/2$ coil which modify the V_5 signals and introduce false effects from non-zero magnetic fields in the target region. If there are no gradients in the magnetic fields we can simplify the above expression,

$$\phi_{diag}^{noGrad} = (Q1 + Q3)/2 - (Q2 + Q4)/2 = \tag{10}$$
$$\theta_{HF5} - \theta_{VF5}$$
$$- 1/2\left(a_1 + b_1 + a_3 + b_3\right)\theta_{HF5}$$
$$+ 1/2\left(a_2 + b_2 + a_4 + b_4\right)\theta_{VF5}$$
$$+ 1/2\left(\left(a_3 + b_3 + a_4 + b_4\right) - \left(a_1 + b_1 + a_2 + b_2\right)\right)\theta_{BTU}$$
$$+ 1/2\left(\left(a_2 + b_2 + a_4 + b_4\right) - \left(a_1 + b_1 + a_3 + b_3\right)\right)\theta_{BLD}.$$

The top and bottom pairs of quadrants both contain horizontal and vertical targets, so if everything is aligned well the total cross-over neutrons from bottom quadrants should equal the number from the top quadrants and then the contribution θ_{BTU} from residual transverse magnetic fields is small. The systematic error from the longitudinal residual field rotation is a different story, since the combination of a larger divergence in the vertical direction and the reduction in cross-over neutrons from the vertical septum conspire to make the cross-over neutrons from the vertical targets much larger than the cross-over neutrons from the horizontal targets. Since the longitudinal field is a problem only after the $\pi/2$ coil, this effect can be reduced by reducing the separation between the end of the $\pi/2$ coil and the start of the output coil. For typical numbers, which one can expect in our apparatus

with an aligned beam and a $2\ cm$ gap after the $\pi/2$ coil, one gets from simulation the following fractions for cross-over neutrons : $a_1 = 0.0148$, $b_1 = 0.0083$, $a_2 = 0.0064$, $b_2 = 0.1952$, $a_3 = 0.0145$, $b_3 = 0.0084$, $a_4 = 0.0066$, $b_4 = 0.1963$, which results in $(Q1 + Q3)/2 - (Q2 + Q4)/2 = 0.9770\,\theta_{HF5} - 0.7978\,\theta_{VF5} + 0.0006\,\theta_{BTU} + 0.1793\,\theta_{BLD}$. Simulations show a $< 2\times10^{-7}$ rad systematic error in a 0.1 mG field. If one adds in addition a 1 m rad neutron beam misalignment then the cross-over neutron fraction from the bottom left ($Q3$) will be more than from the top right ($Q1$), and this difference between the bottom versus top quadrants generates a systematic error from the residual transverse magnetic field. For our assumed residual fields and geometry we get a 2×10^{-6} rad systematic effect.

Magnetic field gradients pose a potentially larger problem. Typical gradients lead to quadrant field differences of less than 10%, so for 6 Å neutrons in a 0.1 mG field, $2\delta_V\theta_{BTU} < 1.5 \times 10^{-4}$ rad. The cross-over neutrons modify this systematic at less than the 10% level. Therefore, while the analysis so far reduces common mode noise, it is not sufficient to remove all magnetic-field related systematic effects to the desired level. To further reduce systematic effects from magnetic fields, we rotate the target by 90° thereby flipping the orientation of the density gradient and thus the signs of the V_5 effects while leaving rotations from magnetic fields unchanged. By taking the difference in ϕ_{diag} (9) before and after a 90° rotation of the target, we eliminate magnetic field rotations while retaining the reduction in common-mode noise,

$$\Phi_m = \frac{\left(\phi_{diag} - \phi'_{diag}\right)}{2} = \left[1 - 1/2\left(a_1 + b_1 + a_3 + b_3\right)\right]\theta_{HF5} \qquad (11)$$
$$- \left[1 - 1/2\left(a_2 + b_2 + a_4 + b_4\right)\right]\theta_{VF5}.$$

Using the cross-over fractions from simulation, we find $\Phi_m \approx 0.98\,\theta_{HF5} - 0.80\,\theta_{VF5}$, and since $\theta_{VF5} < 0.1\,\theta_{HF5}$ we find about a 10% reduction in the desired signal, $\Phi_m \approx 0.9\,\theta_{HF5}$. However, as noted above the subtractions in this last step are done for rotations using different plates, so plate non-uniformities from quadrant to quadrant can generate a systematic error. Consider a mechanical imperfection of the target which generates a 1 mrad angular twist in the plate orientations in quadrant 1 after a 90° target rotation. Our simulations show a systematic effect of almost 1×10^{-6} rad for our assumed residual field values. This is only an issue if the 1 mrad polarization twist in the plates is in the direction opposite the target orientation, e.g. a 1 mrad vertical twist in horizontal target plates.

Another systematic effect in this case can come from differences in the reflectivity of the different pieces of copper, which might not be identical for the two 90° states. Consider a very extreme case in which the copper plates sensitive to V_5 in quadrants/states $Q1$ and $Q3$ possess 100% reflectivity and the different copper plates in the same location in quadrants/states $Q1$ and $Q3$ have completely non-reflective copper plates. In this case one gets a systematic error of 4×10^{-6} rad. Even if such an extreme case were to be realized by some chance between each pair of plates there is no reason that they should be correlated in sign, so one would expect the systematic error from the difference between the average reflective properties of each twelve-plate quadrant to be suppressed by at the very least a factor of $\sqrt{12}$. One can easily perform visual inspection and measurements of the surface roughness of the plates along with neutron reflectometry measurements of the properties of the individual plates themselves to further constrain and suppress this potential source of systematic error.

Table 1 shows our estimates for the sizes of the various forms of systematic error for our target design and measurement methods. Almost all of the systematics are associated with residual magnetic fields coupled with various types of apparatus or beam nonuniformities. The different subtractions enabled by our target design reduce both common-mode noise and systematic errors to the desired level.

Table 1
A list of sources for potential systematic effects in a search for the V_5 interaction using a slow neutron polarimeter in combination with the target design presented in this paper. These estimates all hold for the internal longitudinal and transverse magnetic fields of 0.1 mG assumed. We have included all systematic errors associated with analysis after both modes of target cancellation (diagonal averaging followed by 90° target rotation). All of the dominant sources of systematic error on this list scale with the size of these residual internal fields.

Source	Systematic (rad)
Small angle scattering from ^{4}He atmosphere:	$<1 \times 10^{-7}$
Target mass diamagnetism:	1×10^{-9}
Neutron–atom spin–orbit scattering:	5×10^{-9}
Target magnetic impurities:	$<2 \times 10^{-6}$
Target misalignment:	$<1 \times 10^{-6}$
Target reflectivity differences:	$<1 \times 10^{-6}$

5. Conclusions

The Neutron Spin Rotation collaboration developed a target consisting of alternating plates of different mass materials for use in experiments seeking new spin-dependent interactions using polarized slow neutrons. The four chambers of the target allow cancellation of neutron spin rotations from stray magnetic fields. A Geneva Drive rotates the target such that the plate orientations flip in alternate target states, thereby further canceling magnetic field rotations while isolating rotations from new interactions. The target was used in a recent experiment on the FP12 cold neutron beam at LANSCE, the results of which will be presented in a forthcoming paper.

The sensitivity of this target for this exotic interaction search could be further improved by using a denser nonmagnetic mass such as tungsten or tantalum in place of the copper used in this experiment. The higher density would lead to a greater sensitivity to this possible exotic interaction from the larger number of electrons and nucleons per unit volume in the source. In addition it would be desirable to flatten and polish the surfaces of the test masses exposed to the neutron beam well enough that slow neutrons are guaranteed to undergo specular reflection from the surfaces. This would raise the fraction of neutrons transmitted through the apparatus and increase the sensitivity of the experiment to shorter interaction ranges. The target can be made longer in principle as long as the magnetic shielding can be maintained.

We can estimate the order of magnitude of the sensitivity to the V_5 interaction that could be achieved in a dedicated experiment using a fully optimized target design. Simulations of the neutron spin rotation apparatus for a proposed measurement of parity odd neutron spin rotation in liquid helium (whose statistical error has already been thoroughly analyzed) adapted for this target show that given two months of dedicated beam time it is possible to increase the sensitivity in g_A^2 by 4 orders of magnitude compared to the pioneering work of Piegsa and Pignol. If one can lower the systematic errors further by suppressing the residual longitudinal and transverse magnetic fields in the target region below 100 μG, one could probe neutron axial couplings to matter through an exotic spin 1 boson which are about 13 orders of magnitude weaker than electromagnetism.

References

[1] I. Antoniadis, et al., C. R. Physique, 12 (2011) 755.

[2] M.S. Safronova, D. Budker, D. DeMille, Derek F. Jackson Kimball, A. Derevianko, C.W. Clark, Rev. Mod. Phys. (2017) (in press), arXiv:1710:01833.

[3] B. Dobrescu, I. Mocioiu, J. High Energy Phys. 11 (2006) 005.

[4] F.M. Piegsa, G. Pignol, Phys. Rev. Lett. 108 (2012) 181801.

[5] W.M. Snow, et al., Rev. Sci. Instrum. 86 (2015) 055101.

[6] W.M. Snow, et al., Phys. Rev. C 83 (2011) 022501(R).

[7] H. Yan, W.M. Snow, Phys. Rev. Lett. 110 (2013) 082003.

[8] R. Lehnert, W.M. Snow, H. Yan, Phys. Lett. B 730 (2014) 253; Phys. Lett. B 744 (2015) 415.

[9] R. Lehnert, W.M. Snow, Z. Xiao, R. Xu, Phys. Lett. B 772 (2017) 865.

[10] M.T. Gericke, J.D. Bowman, M.B. Johnson, Phys. Rev. C 78 (2008) 044003.